

# Longitudinal Spin Transfer to the $\Lambda$ Hyperon in Semi-Inclusive Deep-Inelastic Scattering

A. Airapetian,<sup>17</sup> N. Akopov,<sup>30</sup> Z. Akopov,<sup>30</sup> M. Amarian,<sup>8,30</sup> A. Andrus,<sup>16</sup> E.C. Aschenauer,<sup>8</sup> W. Augustyniak,<sup>29</sup> R. Avakian,<sup>30</sup> A. Avetissian,<sup>30</sup> E. Avetissian,<sup>12</sup> P. Bailey,<sup>16</sup> D. Balin,<sup>20</sup> M. Beckmann,<sup>7</sup> S. Belostotski,<sup>20</sup> N. Bianchi,<sup>12</sup> H.P. Blok,<sup>19,28</sup> H. Böttcher,<sup>8</sup> A. Borissov,<sup>15</sup> A. Borysenko,<sup>12</sup> M. Bouwhuis,<sup>16</sup> A. Brüll,<sup>23</sup> V. Bryzgalov,<sup>21</sup> M. Capiluppi,<sup>11</sup> G.P. Capitani,<sup>12</sup> T. Chen,<sup>4</sup> X. Chen,<sup>4</sup> H.C. Chiang,<sup>16</sup> G. Ciullo,<sup>11</sup> M. Contalbrigo,<sup>11</sup> P.F. Dalpiaz,<sup>11</sup> W. Deconinck,<sup>17</sup> R. De Leo,<sup>3</sup> M. Demey,<sup>19</sup> L. De Nardo,<sup>1</sup> E. De Sanctis,<sup>12</sup> E. Devitsin,<sup>18</sup> M. Diefenthaler,<sup>10</sup> P. Di Nezza,<sup>12</sup> J. Dreschler,<sup>19</sup> M. Düren,<sup>14</sup> M. Ehrenfried,<sup>10</sup> A. Elalaoui-Moulay,<sup>2</sup> G. Elbakian,<sup>30</sup> F. Ellinghaus,<sup>6</sup> U. Elschenbroich,<sup>13</sup> R. Fabbri,<sup>19</sup> A. Fantoni,<sup>12</sup> L. Felawka,<sup>26</sup> S. Frullani,<sup>24</sup> A. Funel,<sup>12</sup> G. Gapienko,<sup>21</sup> V. Gapienko,<sup>21</sup> F. Garibaldi,<sup>24</sup> K. Garrow,<sup>26</sup> G. Gavrillov,<sup>7,26,20</sup> V. Gharibyan,<sup>30</sup> O. Grebeniuk,<sup>11</sup> I.M. Gregor,<sup>8</sup> C. Hadjidakis,<sup>12</sup> K. Hafidi,<sup>2</sup> M. Hartig,<sup>14</sup> D. Hasch,<sup>12</sup> W.H.A. Hesselink,<sup>19,28</sup> A. Hillenbrand,<sup>10</sup> M. Hoek,<sup>14</sup> Y. Holler,<sup>7</sup> B. Hommez,<sup>13</sup> I. Hristova,<sup>8</sup> G. Iarygin,<sup>9</sup> A. Ivanilov,<sup>21</sup> A. Izotov,<sup>20</sup> H.E. Jackson,<sup>2</sup> A. Jgoun,<sup>20</sup> R. Kaiser,<sup>15</sup> T. Keri,<sup>14</sup> E. Kinney,<sup>6</sup> A. Kisselev,<sup>6,20</sup> T. Kobayashi,<sup>27</sup> M. Kopytin,<sup>8</sup> V. Korotkov,<sup>21</sup> V. Kozlov,<sup>18</sup> B. Krauss,<sup>10</sup> P. Kravchenko,<sup>20</sup> V.G. Krivokhijine,<sup>9</sup> L. Lagamba,<sup>3</sup> L. Lapikás,<sup>19</sup> A. Laziev,<sup>19,28</sup> P. Lenisa,<sup>11</sup> P. Liebing,<sup>8</sup> L.A. Linden-Levy,<sup>16</sup> W. Lorenzon,<sup>17</sup> H. Lu,<sup>5</sup> J. Lu,<sup>26</sup> S. Lu,<sup>14</sup> X. Lu,<sup>4</sup> B.-Q. Ma,<sup>4</sup> B. Maiheu,<sup>13</sup> N.C.R. Makins,<sup>16</sup> S.I. Manaenkov,<sup>20</sup> Y. Mao,<sup>4</sup> B. Marianski,<sup>29</sup> H. Marukyan,<sup>30</sup> F. Masoli,<sup>11</sup> V. Mexner,<sup>19</sup> N. Meyners,<sup>7</sup> T. Michler,<sup>10</sup> O. Mikloukho,<sup>20</sup> C.A. Miller,<sup>1,26</sup> Y. Miyachi,<sup>27</sup> V. Muccifora,<sup>12</sup> M. Murray,<sup>15</sup> A. Nagaitsev,<sup>9</sup> E. Nappi,<sup>3</sup> Y. Naryshkin,<sup>20</sup> M. Negodaev,<sup>8</sup> W.-D. Nowak,<sup>8</sup> K. Oganessyan,<sup>7,12</sup> H. Ohsuga,<sup>27</sup> A. Osborne,<sup>15</sup> N. Pickert,<sup>10</sup> D.H. Potterveld,<sup>2</sup> M. Raithel,<sup>10</sup> D. Reggiani,<sup>10</sup> P.E. Reimer,<sup>2</sup> A. Reischl,<sup>19</sup> A.R. Reolon,<sup>12</sup> C. Riedl,<sup>10</sup> K. Rith,<sup>10</sup> G. Rosner,<sup>15</sup> A. Rostomyan,<sup>30</sup> L. Rubacek,<sup>14</sup> J. Rubin,<sup>16</sup> D. Ryckbosch,<sup>13</sup> Y. Salomatin,<sup>21</sup> I. Sanjiev,<sup>2,20</sup> I. Savin,<sup>9</sup> A. Schäfer,<sup>22</sup> G. Schnell,<sup>27</sup> K.P. Schüller,<sup>7</sup> J. Seele,<sup>6</sup> R. Seidl,<sup>10</sup> B. Seitz,<sup>14</sup> C. Shearer,<sup>15</sup> T.-A. Shibata,<sup>27</sup> V. Shutov,<sup>9</sup> K. Sinram,<sup>7</sup> W. Sommer,<sup>14</sup> M. Stancari,<sup>11</sup> M. Statera,<sup>11</sup> E. Steffens,<sup>10</sup> J.J.M. Steijger,<sup>19</sup> H. Stenzel,<sup>14</sup> J. Stewart,<sup>8</sup> F. Stinzing,<sup>10</sup> P. Tait,<sup>10</sup> H. Tanaka,<sup>27</sup> S. Taroian,<sup>30</sup> B. Tchuiko,<sup>21</sup> A. Terkulov,<sup>18</sup> A. Trzcinski,<sup>29</sup> M. Tytgat,<sup>13</sup> A. Vandenbroucke,<sup>13</sup> P.B. van der Nat,<sup>19</sup> G. van der Steenhoven,<sup>19</sup> Y. van Haarlem,<sup>13</sup> V. Vikhrov,<sup>20</sup> M.G. Vincter,<sup>1</sup> C. Vogel,<sup>10</sup> J. Volmer,<sup>8</sup> S. Wang,<sup>4</sup> J. Wendland,<sup>25,26</sup> Y. Ye,<sup>5</sup> Z. Ye,<sup>7</sup> S. Yen,<sup>26</sup> B. Zihlmann,<sup>13</sup> and P. Zupranski<sup>29</sup>

(The HERMES Collaboration)

<sup>1</sup>Department of Physics, University of Alberta, Edmonton, Alberta T6G 2J1, Canada

<sup>2</sup>Physics Division, Argonne National Laboratory, Argonne, Illinois 60439-4843, USA

<sup>3</sup>Istituto Nazionale di Fisica Nucleare, Sezione di Bari, 70124 Bari, Italy

<sup>4</sup>School of Physics, Peking University, Beijing 100871, China

<sup>5</sup>Department of Modern Physics, University of Science and Technology of China, Hefei, Anhui 230026, China

<sup>6</sup>Nuclear Physics Laboratory, University of Colorado, Boulder, Colorado 80309-0390, USA

<sup>7</sup>DESY, 22603 Hamburg, Germany

<sup>8</sup>DESY, 15738 Zeuthen, Germany

<sup>9</sup>Joint Institute for Nuclear Research, 141980 Dubna, Russia

<sup>10</sup>Physikalisches Institut, Universität Erlangen-Nürnberg, 91058 Erlangen, Germany

<sup>11</sup>Istituto Nazionale di Fisica Nucleare, Sezione di Ferrara and

Dipartimento di Fisica, Università di Ferrara, 44100 Ferrara, Italy

<sup>12</sup>Istituto Nazionale di Fisica Nucleare, Laboratori Nazionali di Frascati, 00044 Frascati, Italy

<sup>13</sup>Department of Subatomic and Radiation Physics, University of Gent, 9000 Gent, Belgium

<sup>14</sup>Physikalisches Institut, Universität Gießen, 35392 Gießen, Germany

<sup>15</sup>Department of Physics and Astronomy, University of Glasgow, Glasgow G12 8QQ, United Kingdom

<sup>16</sup>Department of Physics, University of Illinois, Urbana, Illinois 61801-3080, USA

<sup>17</sup>Randall Laboratory of Physics, University of Michigan, Ann Arbor, Michigan 48109-1040, USA

<sup>18</sup>Lebedev Physical Institute, 117924 Moscow, Russia

<sup>19</sup>Nationaal Instituut voor Kernfysica en Hoge-Energiefysica (NIKHEF), 1009 DB Amsterdam, The Netherlands

<sup>20</sup>Petersburg Nuclear Physics Institute, St. Petersburg, Gatchina, 188350 Russia

<sup>21</sup>Institute for High Energy Physics, Protvino, Moscow region, 142281 Russia

<sup>22</sup>Institut für Theoretische Physik, Universität Regensburg, 93040 Regensburg, Germany

<sup>23</sup>Thomas Jefferson National Accelerator Facility, Newport News, Virginia 23606, USA

<sup>24</sup>Istituto Nazionale di Fisica Nucleare, Sezione Roma 1, Gruppo Sanità and Physics Laboratory, Istituto Superiore di Sanità, 00161 Roma, Italy

<sup>25</sup>Department of Physics, Simon Fraser University, Burnaby, British Columbia V5A 1S6, Canada

<sup>26</sup>TRIUMF, Vancouver, British Columbia V6T 2A3, Canada

<sup>27</sup>Department of Physics, Tokyo Institute of Technology, Tokyo 152, Japan

<sup>28</sup>Department of Physics and Astronomy, Vrije Universiteit, 1081 HV Amsterdam, The Netherlands

<sup>29</sup>Andrzej Soltan Institute for Nuclear Studies, 00-689 Warsaw, Poland

<sup>30</sup>Yerevan Physics Institute, 375036 Yerevan, Armenia

(Dated: December 2, 2024)

The transfer of polarization from a high-energy positron to a  $\Lambda^0$  hyperon produced in semi-inclusive deep-inelastic scattering has been measured. The data have been obtained by the HERMES experiment at DESY using the 27.6 GeV longitudinally polarized positron beam of the HERA collider and unpolarized gas targets internal to the positron (electron) storage ring. The longitudinal spin transfer coefficient is found to be  $D_{LL'}^\Lambda = 0.11 \pm 0.10$  (stat)  $\pm 0.03$  (syst) at an average fractional energy carried by the  $\Lambda^0$  hyperon  $\langle z \rangle = 0.45$ . The dependence of  $D_{LL'}^\Lambda$  on both the fractional energy  $z$  and the fractional longitudinal momentum  $x_F$  is presented.

In this paper the study of the longitudinal spin transfer from a polarized positron to a  $\Lambda^0$  hyperon produced in the deep-inelastic scattering process is presented. The measurements are sensitive to two unknowns: the spin structure of the lightest hyperon, and the spin-dependent dynamics of the fragmentation process in deep-inelastic scattering.

Given the non-trivial spin structure of the proton [1], it is of interest to consider the spin structure of other baryons. In this respect the  $\Lambda^0$  hyperon is particularly interesting, as it is the lightest strange baryon of the SU(3) spin- $\frac{1}{2}$  octet based on up ( $u$ ), down ( $d$ ), and strange ( $s$ ) quarks. The number density for quarks plus antiquarks of flavor  $f$  in the  $\Lambda^0$  hyperon is denoted below as  $q_f^\Lambda$  ( $f = u, d, s$ ).

In the naive Constituent Quark Model the spin of the  $\Lambda^0$  hyperon is entirely carried by the  $s$  quark:  $\Delta q_s^\Lambda = 1$ , while the  $ud$  pair is in a spinless (singlet) state, i.e.,  $\Delta q_u^\Lambda = \Delta q_d^\Lambda = 0$ . Here  $\Delta q_f^\Lambda \equiv q_f^{\Lambda+} - q_f^{\Lambda-}$ , where  $q_f^{\Lambda+}$  and  $q_f^{\Lambda-}$  describe the net alignment of the quark spins along (+) or against (−) the hyperon spin direction, respectively, while the unpolarized number density is  $q_f^\Lambda \equiv q_f^{\Lambda+} + q_f^{\Lambda-}$ . Alternatively, one can use SU(3)-flavor symmetry in conjunction with the experimental results on the proton to estimate the first moments of the helicity-dependent quark distributions in the  $\Lambda^0$  hyperon. Using such assumptions Burkardt and Jaffe found  $\Delta q_u^\Lambda = \Delta q_d^\Lambda = -0.23 \pm 0.06$  and  $\Delta q_s^\Lambda = 0.58 \pm 0.07$  [2]. According to this estimate, the spins of the  $u$  and  $d$  quarks and antiquarks are directed predominantly opposite to the spin of the  $\Lambda^0$  hyperon resulting in a weak but non-zero net polarization. If such an SU(3)-flavor rotation (see Eq. 3 of Ref. [3], for example) is applied to the recent semi-inclusive data on the nucleon [4], the values  $\Delta q_u^\Lambda = \Delta q_d^\Lambda = -0.09 \pm 0.06$  and  $\Delta q_s^\Lambda = 0.47 \pm 0.07$  are obtained instead, favoring a much smaller polarization of the  $u$  and  $d$  quarks and antiquarks. A lattice-QCD calculation [3] also finds small light-quark polarizations,  $\Delta q_u^\Lambda = \Delta q_d^\Lambda = -0.02 \pm 0.04$  and  $\Delta q_s^\Lambda = 0.68 \pm 0.04$ . Finally, other authors [5, 6, 7] have employed phenomenological models to explore the dependence of  $\Delta q_f^\Lambda(x)$  on the Bjorken scaling variable  $x$ . These models predict a large positive polarization of the  $u$  and  $d$  quarks in the kinematic region  $x > 0.3$ .

As it is not experimentally feasible to scatter directly from hyperon targets, another probe of hyperon spin structure must be found to address these model predictions. One possibility, as suggested in Ref. [8], is to study hyperons produced in the *final state* of the deep-inelastic scattering (DIS) process, and to employ the fragmentation process by which they are formed as a “polarimeter” for the quarks within. More precisely, when a longitudinally-polarized lepton beam is scattered at high energies from a nucleon target, angular momentum conservation dictates that quarks of a particular spin orientation participate predominantly in the interaction. The outgoing struck quark is thus polarized, and hyperons produced from its fragmentation may “remember” its spin orientation and carry a longitudinal polarization themselves. Formally such a correlation may be expressed in terms of a spin-dependent fragmentation function, denoted  $G_{1,f}^\Lambda(z)$  in the notation of Ref. [9], where  $z$  is the fractional energy of the  $\Lambda^0$  hyperon. (This fragmentation function has often appeared in the literature with different symbols, most notably as  $\Delta D^\Lambda(z)$  in Ref. [5] or as  $\Delta \hat{q}_\Lambda(z)$  in Ref. [8].) The magnitude of this spin-dependent fragmentation function is sensitive to quark helicity conservation and to the correlation between quark spins in the complex fragmentation process. It is also sensitive to the spin structure of the produced  $\Lambda^0$  hyperon, provided the amount of  $\Lambda^0$ s produced from unpolarized quarks in the process of color-string breaking or from the decay of heavier hyperons with different spin structure is not significant.

The polarization of final-state  $\Lambda^0$  hyperons can be measured via the weak decay channel  $\Lambda^0 \rightarrow p\pi^-$  through the angular distribution of the final-state particles:

$$\frac{dN}{d\Omega_p} \propto 1 + \alpha \vec{P}_\Lambda \cdot \hat{k}_p. \quad (1)$$

Here  $\frac{dN}{d\Omega_p}$  is the angular distribution of the protons,  $\alpha = 0.642 \pm 0.013$  is the asymmetry parameter of the parity-violating weak decay,  $\vec{P}_\Lambda$  is the polarization of the  $\Lambda^0$ , and  $\hat{k}_p$  is the unit vector along the proton momentum in the rest frame of the  $\Lambda^0$ . Because of the parity-violating nature of this decay, the proton is preferentially emitted along the spin direction of its parent, thus offering access

to spin degrees of freedom in the deep-inelastic scattering final state.

Longitudinal spin transfer to  $\Lambda^0$  hyperons has previously been explored by the LEP experiments OPAL and ALEPH at an energy corresponding to the  $Z^0$  pole [11, 12]. In these experiments the  $\Lambda^0$  hyperons are predominantly produced via the decay  $Z^0 \rightarrow s\bar{s}$ , in which the primary strange quarks from the decay are strongly (and negatively) polarized at the level of  $-91\%$ . The OPAL and ALEPH data show a  $\Lambda^0$  polarization of about  $-30\%$  at  $z > 0.3$ . It rises in magnitude as  $z$  increases. Here,  $z$  is the ratio between the energy of the  $\Lambda^0$  and that of the primary (fragmenting) quark. The LEP data have been described using a Lund-based Monte Carlo model along with the following hypotheses, originally postulated in Ref. [13]: (1) that the primary quarks produced in the  $Z^0$  decay retain their helicity throughout the fragmentation process, (2) that the quarks produced from color-string breaking have no preferred spin direction, and (3) that the spin structure of the produced hyperons can be adequately described by the Constituent Quark Model.

In contrast to the LEP experiments, production of  $\Lambda^0$  hyperons in deep-inelastic scattering of leptons from nucleons is dominated by scattering from  $u$  and  $d$  quarks. In the NOMAD experiment [14], the production of  $\Lambda^0$  hyperons was studied in  $\nu_\mu$  charged-current interactions. Also in contrast to the LEP experiments, the NOMAD data are concentrated in the kinematic domain  $x_F < 0$  corresponding to the so-called target fragmentation region. (The Feynman- $x$  variable is defined in the standard way as  $x_F \equiv p_{\parallel}/p_{\parallel max}$ . Here  $p_{\parallel}$  is the projection of the hadron momentum on the virtual-photon ( $\gamma^*$ ) or  $W$ -boson ( $W^*$ ) direction,  $p_{\parallel max}$  is its maximum possible value, and all quantities are evaluated in the  $\gamma^*N$  or  $W^*N$  center-of-mass system, where  $N$  is the target nucleon). A non-zero longitudinal  $\Lambda^0$  polarization was observed at  $x_F < 0$  while at  $x_F > 0$  the polarization was found to be compatible with zero [14]. A mechanism giving rise to non-zero polarization values in the region  $x_F < 0$  is described in Ref. [15].

Using charged lepton beams, only two measurements of longitudinal  $\Lambda^0$  polarization in deep-inelastic scattering have been reported to date. The E665 collaboration [16] measured a negative polarization by using a polarized muon beam of 470 GeV. The statistical accuracy of the E665 experiment is rather limited, however, as only 750  $\Lambda^0$  events were identified.

Results on the longitudinal spin transfer in deep-inelastic scattering were also reported by the HERMES collaboration [17]. These data were obtained using the 27.6 GeV polarized positron beam of the HERA  $e$ - $p$  collider, and were collected during the years 1996 and 1997. After subtraction of the background and application of several kinematic requirements, about 2,000  $\Lambda^0$  hyperons were reconstructed. The longitudinal spin-

transfer coefficient, which is defined below in Eq. 2, for forward ( $x_F > 0$ )  $\Lambda^0$  production was measured to be  $D_{LL'}^{\Lambda} = 0.11 \pm 0.17$  (stat)  $\pm 0.03$  (sys), at an average fractional energy  $\langle z \rangle = 0.45$ . In deep-inelastic scattering, the fractional energy  $z$  is defined as  $z = E_{\Lambda}/\nu$ , where  $E_{\Lambda}$  is the energy of the  $\Lambda^0$  hyperon,  $\nu = E - E'$ , and  $E$  and  $E'$  represent the energy of the primary and scattered lepton, respectively. Since the energy of the current (struck) quark after absorption of the virtual photon is very close to  $\nu$ , the value  $z$  in deep-inelastic scattering is practically the same as that in the LEP experiments discussed above, thus allowing comparison of both results.

Recently, the CLAS experiment at Jefferson Laboratory measured large spin transfers from polarized 2.6 GeV beam electrons to  $\Lambda^0$ s produced in the exclusive reaction  $\bar{e}p \rightarrow e'K^+\bar{\Lambda}$  [18]. However, due to the exclusive nature of this reaction and the low energy of the experiment, these data cannot be readily compared with results from high-energy deep-inelastic scattering.

The HERMES results presented in this paper surpass the data of Ref. [17] in statistical precision. The new data were mostly accumulated during the very successful HERA data-taking period in the years 1999-2000. In this period a Ring Imaging Čerenkov (RICH) detector [19] was used for hadron identification. The old HERMES  $D_{LL'}^{\Lambda}$  data collected during the years 1996 and 1997 (Ref. [17]) are included in the analysis, leading to a total of almost 8,000  $\Lambda^0$  events.

As compared to previous measurements, the additional data allow the exploration of the  $z$ -dependence of the spin transfer  $D_{LL'}^{\Lambda}$ . This is of particular interest, as the  $z$ -dependence provides a crucial test for the dominant  $\Lambda^0$ -formation mechanism. Some models actually predict a very pronounced  $z$ -dependence for  $\Lambda^0$  polarization. The data were also binned in the variable  $x_F$ , enabling a comparison of all the available data collected in the target- and current-fragmentation regions by the HERMES, NOMAD, and E665 experiments.

The paper is organized as follows. Section 2 summarizes the spin transfer in the framework of the quark-parton model. Having introduced the relevant variables in section 2, section 3 is devoted to a brief description of the experiment and a discussion of the analysis techniques. The experimental results are presented and discussed in section 4, and section 5 concludes the paper with summary remarks.

## II. LONGITUDINAL SPIN TRANSFER

The dominant mechanism for semi-inclusive production of longitudinally polarized  $\Lambda^0$  hyperons in polarized deep-inelastic scattering is sketched in Fig. 1. It should be noted that at the moderate energy of the HERMES experiment the distinction between the current and target fragmentation domain is not very sharp. The condi-

tion  $x_F > 0$  only selects  $\Lambda^0$  particles moving forward in the  $\gamma^*p$  rest frame but does not exclude a contribution from the target remnant. Nevertheless, with this requirement imposed the remnant contribution is assumed to be reduced.

As indicated by the arrows in Fig. 1, a beam positron of positive helicity emits a polarized virtual photon (denoted  $\gamma^*$ ) which is absorbed by a quark  $q$  in the target proton with the spin direction opposite to that of  $\gamma^*$ . This fixes the spin orientation of the struck quark: after the spin-1 photon is absorbed, the outgoing quark has the same helicity as the virtual photon.

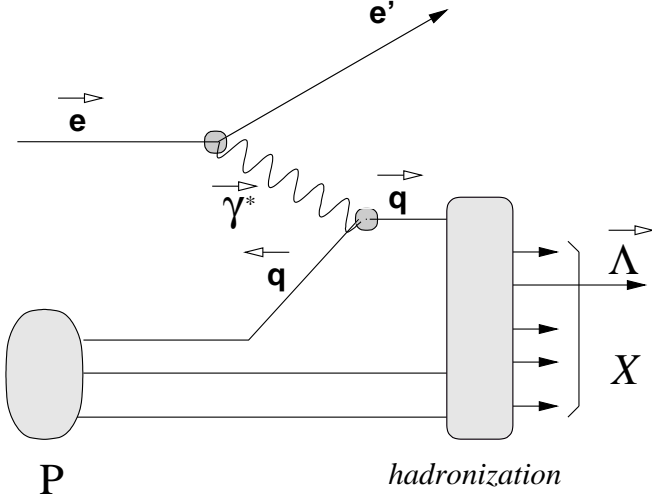


FIG. 1: The single-quark scattering mechanism leading to  $\Lambda^0$  production in polarized deep-inelastic positron scattering.

More precisely, if the longitudinal polarization of the beam is given by  $P_b$  and the target is unpolarized, the struck quark will acquire a polarization  $P_q = P_b D(y)$  directed along its momentum. Here  $y = \nu/E$  is the fractional energy carried by the photon and  $D(y) \simeq [1 - (1 - y)^2]/[1 + (1 - y)^2]$  is the depolarization factor taking into account the loss of polarization of the virtual photon as compared to that of the incident positron. Positive beam polarization  $P_b$  refers to the case when the beam positron has preferentially positive helicity in the target rest frame. The component of the polarization transferred along the direction  $L'$  from the virtual photon to the produced  $\Lambda^0$  is given by

$$P_{L'}^\Lambda = P_b D(y) D_{LL'}^\Lambda, \quad (2)$$

where  $L$  is the primary quantization axis, directed along the virtual photon momentum. The spin transfer coefficient  $D_{LL'}^\Lambda$  in Eq. 2 describes the probability that the polarization of the struck quark is transferred to the  $\Lambda^0$  hyperon along the secondary quantization axis  $L'$ . In principle, the spin transfer can be studied experimentally for any direction of the  $L'$  axis. Interesting information

on the dynamics of the reaction and on the mechanism of spin transfer from the struck quark to the produced  $\Lambda^0$  can be obtained by measuring the longitudinal component of the transferred polarization. Different authors differ in their definition of the direction of the longitudinal component [8, 9, 10]: choices for the  $L'$  direction include the directions of the momentum of the virtual-photon, of the produced  $\Lambda^0$ , and of the lepton beam. As described in later sections, two of these choices were explored in this analysis and gave fully-compatible results.

In the notation of [9], the longitudinal spin-transfer from the virtual photon to the  $\Lambda^0$  hyperon in DIS is expressed in terms of a spin-transfer fragmentation function  $G_{1,f}$ :

$$D_{LL'}^\Lambda(x, z, Q^2) = \frac{\sum_f e_f^2 q_f(x, Q^2) G_{1,f}^\Lambda(z, Q^2)}{\sum_f e_f^2 q_f(x, Q^2) D_{1,f}^\Lambda(z, Q^2)}. \quad (3)$$

Here,  $e_f$  is the charge of the quark (or antiquark), and the sum is taken over quark (antiquark) flavors  $f$ . The function  $q_f(x, Q^2)$  is the number density of a quark  $f$  in the target, and  $x = Q^2/2M_p\nu$  represents the Bjorken scaling variable, where  $M_p$  is the proton mass and  $Q^2$  is the negative four-momentum transfer squared.

In Eq. 3,  $D_{1,f}^\Lambda(z, Q^2)$  is the familiar spin-independent fragmentation function describing the number density for  $\Lambda^0$  production from a primary quark  $f$ . Less familiar is the spin-dependent fragmentation function  $G_{1,f}^\Lambda$  [9]. It is defined as  $G_{1,f}^\Lambda = D_{1,f+}^{\Lambda+} - D_{1,f+}^{\Lambda-}$ , while the unpolarized fragmentation function is  $D_{1,f}^\Lambda = D_{1,f+}^{\Lambda+} + D_{1,f+}^{\Lambda-}$ . Here, the symbols  $D_{1,f+}^{\Lambda+}$  or  $D_{1,f+}^{\Lambda-}$  are used to denote the fragmentation functions for a quark of helicity  $+$  to produce a  $\Lambda^0$  of helicity  $+$  or  $-$ , respectively. It is assumed that  $D_{1,f+}^{\Lambda+} = D_{1,f-}^{\Lambda-}$  and  $D_{1,f+}^{\Lambda-} = D_{1,f-}^{\Lambda+}$ .

Both the quark-density distributions and the fragmentation functions in Eq. 3 are slowly varying with  $Q^2$ , so that to a good approximation

$$D_{LL'}^\Lambda(x, z, Q^2) \simeq D_{LL'}^\Lambda(x, z)_{Q^2=\langle Q^2 \rangle},$$

where  $\langle Q^2 \rangle$  is the average value of  $Q^2$ . After integrating over  $x$  it reads:

$$\begin{aligned} D_{LL'}^\Lambda(z) &\simeq \sum_f \frac{G_{1,f}^\Lambda(z)}{D_{1,f}^\Lambda(z)} \int \frac{e_f^2 q_f(x) D_{1,f}^\Lambda(z)}{\sum_{f'} e_{f'}^2 q_{f'}(x) D_{1,f'}^\Lambda(z)} dx \\ &= \sum_f D_{LL',f}^\Lambda(z) \omega_f^\Lambda(z). \end{aligned} \quad (4)$$

Here the quantity  $D_{LL',f}^\Lambda$  denotes the *partial* spin transfer from a struck quark of flavor  $f$  to a  $\Lambda^0$  hyperon:

$$D_{LL',f}^\Lambda(z) = \frac{G_{1,f}^\Lambda(z)}{D_{1,f}^\Lambda(z)} \equiv \frac{D_{1,f+}^{\Lambda+}(z) - D_{1,f+}^{\Lambda-}(z)}{D_{1,f+}^{\Lambda+}(z) + D_{1,f+}^{\Lambda-}(z)}. \quad (5)$$

The purity  $\omega_f^\Lambda(z)$  in Eq. 4 is the net probability that a  $\Lambda^0$  was produced at average  $Q^2 \approx \langle Q^2 \rangle$  with a fractional

energy  $z$  after absorption of a virtual photon by a quark of flavor  $f$ . It is obvious that

$$\sum_f \omega_f^\Lambda(z) = 1. \quad (6)$$

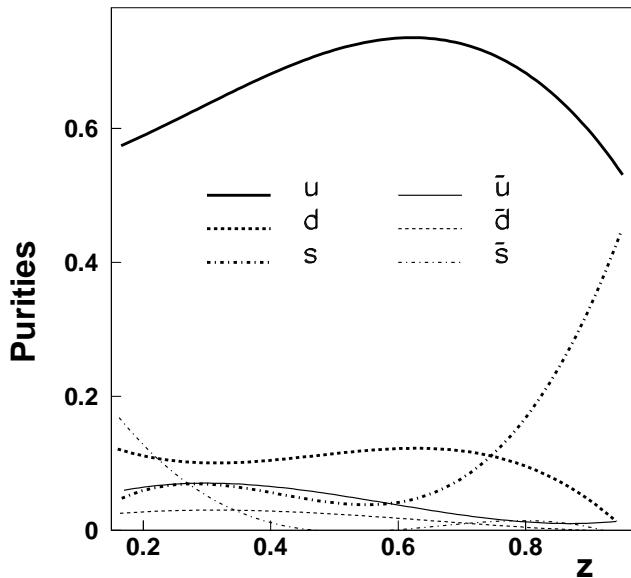


FIG. 2: Purities for  $\Lambda^0$  production from the proton target within the HERMES acceptance, calculated separately for quarks and antiquarks of various flavors at  $x_F > 0$  with  $\langle Q^2 \rangle = 2.41 \text{ GeV}^2$ .

The purities depend on unpolarized quantities only, and can be obtained from a Monte Carlo model. Fig. 2 shows purity distributions for quarks of various flavors calculated using the JETSET Monte Carlo for  $\Lambda^0$  production from a proton target. The calculations have been done in the current fragmentation region ( $x_F > 0$ ) for HERMES kinematics. The strength of the electromagnetic interaction between a lepton and a quark is proportional to the square of the quark charge  $e_f$ . Hence  $\Lambda^0$  production in electron (or muon) induced deep-inelastic scattering is dominated by scattering from  $u$  quarks, as shown in Fig. 2. The strange quark plays a minor role at moderate  $z$ . Its contribution is sharply increasing only at very high  $z$ , which is difficult to access experimentally.

It is apparent that the spin-transfer fragmentation function  $G_{1,f}^\Lambda$  is expected to be related to the spin structure of the  $\Lambda^0$  hyperon. For example, under the assumptions that the produced hyperon actually contains the struck quark of flavor  $f$ , that it was produced directly from fragmentation (and not from the decay of a heavier hyperon), and that the original helicity of the quark is preserved during the fragmentation process, the partial spin-transfer coefficient has been estimated using a

theoretical model of the  $\Lambda^0$  spin structure to be [20]

$$D_{LL',f}^\Lambda \equiv \frac{G_{1,f}^\Lambda}{D_{1,f}^\Lambda} \simeq \frac{\Delta q_f^\Lambda}{q_f^\Lambda}. \quad (7)$$

Here,  $\Delta q_f^\Lambda/q_f^\Lambda$  may be interpreted as the average polarization of quarks of flavor  $f$  in the  $\Lambda^0$  hyperon, and  $D_{LL',f}^\Lambda$  as the partial spin transfer averaged over production kinematics. Despite the number of simplifying assumptions that have been made in deriving Eq. 7, it is a useful starting point for developing a qualitative understanding of  $D_{LL'}^\Lambda$ .

It must be noted that Eq. 7 can be also obtained as a consequence of the reciprocity relation based on crossing symmetry [21]. Strictly speaking, however, it is expected to be valid only at large values of the Bjorken scaling variable for the  $\Lambda^0$ ,  $x_\Lambda$ , and of  $z$ , providing an exact link between the spin-transfer coefficient and spin structure of the  $\Lambda^0$  baryon in the limit of  $x_\Lambda \rightarrow 1$ ,  $z \rightarrow 1$ .

Because of strong  $u$ -quark dominance, one would expect that for electron (or muon) deep-inelastic scattering

$$D_{LL'}^\Lambda \approx \Delta q_u^\Lambda/q_u^\Lambda. \quad (8)$$

This relation is not changed by the  $d$ -quark contribution to the extent that  $\Delta q_u^\Lambda/q_u^\Lambda = \Delta q_d^\Lambda/q_d^\Lambda$  because of isospin symmetry. Further, as shown in Fig. 2, the  $u/d$ -quark dominance approximation in Eq. 8 is exact for at least 70% of the events within the accessible  $z$ -range, reaching almost 90% at intermediate  $z$  values of around 0.6. In the Constituent Quark Model, the net  $u$ -quark polarization in the  $\Lambda^0$  is zero. As explained in the introduction, the use of recent HERMES results on proton structure gives a small negative  $\Delta q_u^\Lambda$  of  $-0.09 \pm 0.06$  [4], while a lattice QCD calculation gives  $-0.02 \pm 0.04$  [3]. The spin transfer to  $\Lambda^0$  hyperons in deep-inelastic scattering might thus be, in principle, a probe of the small non-strange components of the  $\Lambda^0$  spin structure. This is quite different from the case of  $e^+e^- \rightarrow \Lambda^0 X$ , where the  $s$ -quark plays a dominant role.

### III. EXPERIMENT AND EVENT SELECTION

The  $\Lambda^0$  electroproduction data presented in this paper were accumulated by the HERMES experiment at DESY. In this experiment, the 27.6 GeV longitudinally-polarized positron beam [22] of the HERA  $e$ - $p$  collider is passed through an open-ended tubular storage cell into which polarized or unpolarized target atoms in undiluted gaseous form are continuously injected. The HERMES detector is described in detail in Ref. [23].

The data presented here were recorded during two two-year periods: 1996-1997 and 1999-2000 using positron beams. A variety of unpolarized target gases were used in the analysis. Most of the data were collected from

hydrogen and deuterium, but  $^3\text{He}$ ,  $^4\text{He}$ ,  $^{14}\text{N}$ ,  $^{20}\text{Ne}$  and  $^{84}\text{Kr}$  targets were also included, and the data from all targets were combined.

The scattered positrons and the  $\Lambda^0$  decay products were detected by the HERMES spectrometer in the polar-angle range from 40 to 220 mrad. A positron trigger was formed from a coincidence between three scintillator hodoscope planes and a lead-glass calorimeter. The trigger required a minimum energy deposit in the calorimeter of 3.5 GeV for the data employed in this analysis. Charged-particle identification was based on the responses of four detectors; a threshold Čerenkov counter, a transition-radiation detector, a preshower scintillator hodoscope, and a lead-glass calorimeter. Altogether, the particle identification (PID) system provides an average positron identification efficiency of 99% with a hadron contamination of less than 1%. In 1998 the threshold Čerenkov counter was replaced by the Ring Imaging Čerenkov (RICH) detector [19], providing an improved hadron identification capability.

The  $\Lambda^0$  hyperons were identified in the analysis through their  $p\pi^-$  decay channel. Events were selected by requiring the presence of at least three reconstructed tracks: a positron track and two hadron candidates of opposite charge. If more than one positive or negative hadron was found in one event, all possible combinations of positive and negative hadrons were used. The requirements  $Q^2 > 0.8 \text{ GeV}^2$  and  $W > 2 \text{ GeV}$  were imposed on the positron kinematics to ensure that the events originated from the deep-inelastic scattering domain. Here  $W = \sqrt{M_p^2 + 2M_p\nu - Q^2}$  is the invariant mass of the photon-nucleon system. In addition, the requirement  $y = 1 - E'/E < 0.85$  was imposed as the minimum value of  $E'$  was given by the calorimeter threshold of 3.5 GeV.

The kinematics of the  $\Lambda^0$  decay products detected by the HERMES spectrometer is such that the proton momentum is always much higher than that of the pion. These low-momentum pions are often bent so severely in the spectrometer magnet that they fail to reach the tracking chambers and PID detectors in the backward half of the spectrometer. However, it is possible to evaluate the momentum of such “short tracks” using the hits recorded by the HERMES Magnet Chambers, a series of proportional chambers located between the poles of the spectrometer magnet [24]. The acceptance for  $\Lambda^0$  hyperons can be increased by almost a factor of two by including in the analysis the decay pions detected as short tracks. As the great majority of low-momentum particles produced in deep-inelastic scattering are pions, particle identification is not essential for these tracks. By comparison, particle identification of the decay proton is important for background reduction, and PID is crucial in the identification of the scattered lepton. Candidates for these particles were therefore required to be “long tracks”, i.e., tracks passed through all detectors of the spectrometer.

Two spatial vertices were reconstructed for each event by determining the intersection (i.e., point of closest approach) of pairs of reconstructed tracks. The primary (production) vertex was determined from the intersection of the beamline and the scattered beam lepton, while the secondary (decay) vertex was determined from the intersection of the proton and pion tracks. In both cases, the distance of closest approach was required to be less than 1.5 cm. All tracks were also required to satisfy a series of fiducial-volume cuts designed to avoid the inactive edges of the detector. For tracks fulfilling these requirements the invariant mass of the hadron pair was evaluated, under the assumption that the high-momentum leading hadron is the proton while the low-momentum hadron is the pion. There is a clear  $\Lambda^0$  peak even without background suppression cuts. This spectrum is displayed in Fig. 3, left panel.

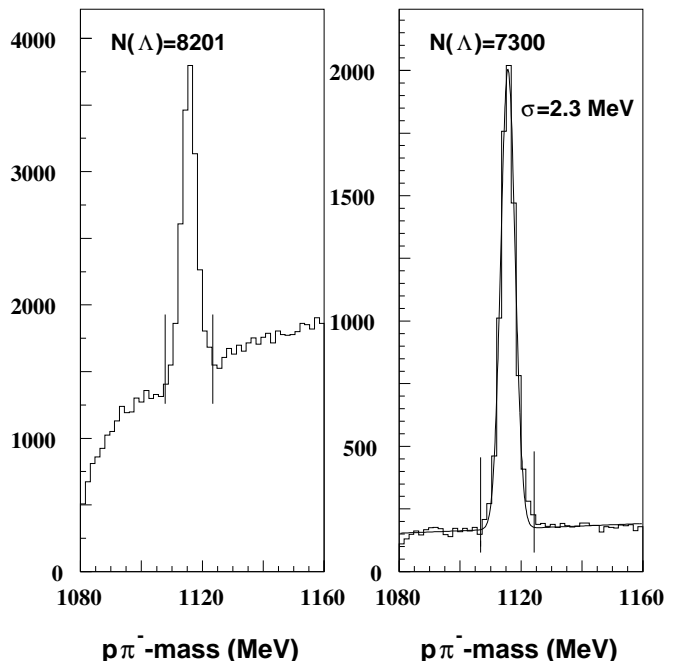


FIG. 3: The yield of semi-inclusively produced  $\Lambda^0$  hyperons in deep-inelastic scattering. The left (right) panel shows the invariant-mass spectrum before (after) the application of background suppression cuts. The vertical lines show the boundaries at  $\pm 3.3\sigma$ . The spectra include essentially all data recorded from unpolarized targets by the HERMES spectrometer in the years 1996 – 1997 and 1999 – 2000, corresponding to a yield of  $30.3 \times 10^6$  inclusive deep-inelastic scattering events.

In order to suppress background, two different approaches were taken, depending on the availability of the RICH detector. For the data taken prior to 1998, hadron pairs with leading pions were suppressed with

the help of the threshold Čerenkov counter. In addition, hadrons emitted from the primary vertex were suppressed by introducing a vertex separation requirement of  $z_2 - z_1 > 10$  cm, with  $z_1$  and  $z_2$  representing the coordinates of the primary and secondary vertex positions along the beam direction. In later years, with the RICH detector available, no vertex separation cut was used. In this case, protons with momenta larger than 4 GeV (which applies to 75% of all protons from  $\Lambda^0$  decay) could be distinguished from lighter hadrons, providing sufficient background reduction. Without background suppression, 8,200  $\Lambda^0$  events were extracted from all unpolarized data, while the final data sample, with all requirements imposed, contained 7,300  $\Lambda^0$  events. These numbers were obtained by integrating the  $\Lambda^0$  peak between the boundaries  $\pm 3.3\sigma$ , shown in Fig. 3 with the vertical lines, and subtracting the background.

An average beam polarization of about 55% was typical during data taking. Reversal of the polarization direction was performed three times during the 1996-1997 data taking period, but more frequently thereafter. Similar amounts of data were recorded in each beam helicity state.

Two independent polarimeters were used to measure the beam polarization. They used similar techniques based on laser Compton backscattering. The polarimeter TPOL [25] measured the transverse beam polarization outside the HERMES spin rotators, while the polarimeter LPOL [26], located between the spin rotators, measured the longitudinal polarization at the HERMES interaction point. In practice, the value measured by the LPOL was taken, except for periods where only the TPOL was in operation. The fractional systematic uncertainty of the beam polarization measured by the LPOL was typically less than 2%. For the TPOL measurements, it was less than 3.5%.

## IV. EXPERIMENTAL RESULTS

### A. Extraction of $D_{LL'}^\Lambda$

Combining Eqs. 1 and 2, the angular distribution of decay protons may be expressed in terms of the longitudinal spin-transfer coefficient  $D_{LL'}^\Lambda$ :

$$\frac{dN}{d\Omega_p} \propto 1 + \alpha P_b D(y) D_{LL'}^\Lambda \cos \Theta_{pL'}. \quad (9)$$

Here  $\Theta_{pL'}$  is the angle between the proton momentum in the  $\Lambda^0$  rest frame and the  $\Lambda^0$  spin quantization axis  $L'$ . Proceeding from the discussion in section II, two choices of the spin-quantization axis  $L'$  for the final-state  $\Lambda^0$  are considered in this analysis:

Axis 1: along the direction of the virtual photon momentum in the  $\Lambda^0$  rest frame;

Axis 2: along the direction of  $\Lambda^0$  momentum (not affected by the relativistic transformation to the  $\Lambda^0$  rest frame).

For HERMES kinematics, unlike the case of deep-inelastic scattering at very high energies, axes 1 and 2 are typically not collinear. It has been found that the angle between axis 1 and axis 2 varies over a wide range with an average value of 35 degrees in the  $\Lambda^0$  rest frame. Hence, both possibilities of  $D_{LL'}^\Lambda$  reconstruction (axis 1 and axis 2) were considered in the analysis.

The HERMES spectrometer is a forward detector with a limited acceptance for the reconstruction of  $\Lambda^0$  hyperons. The efficiency to detect a pion from  $\Lambda^0$  decay depends strongly on its momentum in the laboratory frame, and on its decay angle ( $\pi - \Theta_{pL'}$ ) in the  $\Lambda^0$  rest frame, resulting in a forward ( $\cos \Theta_{pL'} > 0$ ) / backward ( $\cos \Theta_{pL'} < 0$ ) asymmetric acceptance function.

In order to cancel this acceptance effect, the spin transfer to the  $\Lambda^0$  has been determined by combining the two data sets measured with opposite beam polarizations into one helicity-balanced data sample, in which the luminosity-weighted average beam polarization for the selected data is

$$\overline{P_b} \equiv \frac{1}{L} \int P_b dL = 0. \quad (10)$$

Here  $L = \int dL$  is the integrated luminosity.

A detailed derivation based on the method of maximum likelihood leads to the relation [27]:

$$D_{LL'}^\Lambda = \frac{1}{\alpha P_b^2} \cdot \frac{\sum_{i=1}^{N_\Lambda} P_{b,i} D(y_i) \cos \Theta_{pL'}^i}{\sum_{i=1}^{N_\Lambda} D^2(y_i) \cos^2 \Theta_{pL'}^i}. \quad (11)$$

Here,  $\overline{P_b^2} \equiv (\frac{1}{L}) \int P_b^2 dL$  is the luminosity-weighted average of the square of the beam polarization.

The  $\Lambda^0$  polarization was studied as a function of certain kinematic variables. Using Eq. 11, the spin transfer  $\hat{D}_{LL'}^\Lambda$  was calculated for the events within the  $\Lambda^0$  invariant-mass peak (between the boundaries  $\pm 3.3\sigma$ ) in each kinematic bin. The fraction of background events  $\epsilon = \frac{N_{bgr}}{N_\Lambda + N_{bgr}}$  within the peak was typically of order 20%. The spin transfer for the background  $D_{LL'bgr}^\Lambda$  was determined from the events above and below the peak outside of the  $\pm 3.3\sigma$  invariant-mass window. In order to obtain the final result for the net  $\Lambda^0$  events, the spin transfer within the  $\Lambda^0$  peak was corrected for this background contribution in each kinematic bin as

$$D_{LL'}^\Lambda = \frac{\hat{D}_{LL'}^\Lambda - \epsilon D_{LL'bgr}^\Lambda}{1 - \epsilon}. \quad (12)$$

It should be noted that the sideband (background) spin-transfer coefficient  $D_{LL'bgr}^\Lambda$  in Eq. 12 was always consistent with zero.

	96-97	99-00	All Data
$\langle D_{LL'}^{\Lambda} \rangle$ , axis 1	$0.12 \pm 0.17$	$0.12 \pm 0.12$	$0.12 \pm 0.10$
$\langle D_{LL'}^{\Lambda} \rangle$ , axis 2	$0.13 \pm 0.17$	$0.10 \pm 0.13$	$0.11 \pm 0.10$
$\int L$ , pb $^{-1}$	226.9	330.5	557.4
$N_{\Lambda}$	2,452	4,294	6,746
$\langle z \rangle$	0.44	0.46	0.45
$\langle x_F \rangle$	0.29	0.31	0.30

TABLE I: Results for  $D_{LL'}^{\Lambda}$  averaged over kinematics with the requirement  $x_F > 0$  imposed. (Note that the total number of  $\Lambda^0$  events  $N_{\Lambda}$  is reduced as compared with that in Fig. 3, right panel, due to this requirement.) The quoted uncertainties are statistical only. The systematic uncertainties are on the level of  $\pm 0.03$  as discussed in the text.

### B. $D_{LL'}^{\Lambda}$ averaged over kinematics

Table I presents the results for  $D_{LL'}^{\Lambda}$  averaged over HERMES kinematics with the requirement  $x_F > 0$  imposed. As shown in the table, the results from the 1996-1997 data set (where the RICH detector was not present) are fully compatible with those from the 1999-2000 data set. Hereafter, only results from the combined data set are considered.

Two sources of systematic uncertainties were identified and evaluated. First, the helicity-balanced analysis method outlined above relies on an accurate normalization of the data samples with positive and negative beam helicity. In order to estimate the associated systematic uncertainty, the luminosity of each sample was determined using two different methods: (1) using the number of inclusive deep-inelastic scattering events found in each sample, and (2) using the number of semi-inclusive deep-inelastic scattering events containing an oppositely-charged hadron pair with invariant mass outside the  $\Lambda^0$  peak. In both cases the spectrometer acceptance is assumed to be unaffected by the reversal of the beam polarization. The inclusive deep-inelastic scattering cross section is independent of the beam polarization as the target is unpolarized. The same is true for any semi-inclusive cross-section as long as it is fully integrated over the angular distribution of the final-state hadrons. The spin-transfer results were found to differ by less than 0.03 when the two normalization methods were used, and a systematic uncertainty of  $\pm 0.015$  was assigned to account for this difference.

Second, as a further check of the systematic uncertainties involved in the extraction procedure, the spin transfer coefficient was determined for oppositely-charged hadron pairs ( $h^+h^-$ ), where the identity of the hadrons was not restricted. The invariant mass of each pair was calculated assuming it was a  $p\pi^-$  pair with a mass lying outside the  $\Lambda^0$  mass window shown in Fig. 3, left panel. Using this background sample,  $D_{LL'}^{\Lambda}$  was found

to be compatible with zero:  $0.005 \pm 0.014$  using axis 1 and  $0.003 \pm 0.014$  using axis 2. Nevertheless, a  $\pm 0.014$  contribution was added to the overall systematic uncertainty to account for the statistical limitations of this false-asymmetry test.

The systematic uncertainty of  $D_{LL'}^{\Lambda}$  due to beam polarization measurements was estimated to be less than 0.002. Other uncertainties related to smearing effects, choice of the background-suppression procedure, and corrections for the background contribution (Eq. 12) were also found to be small.

Based on these results, one can conclude that the systematic uncertainty on the spin-transfer coefficient is dominated by the normalization uncertainty of the helicity-balanced analysis method ( $\pm 0.015$ ) and possible experimental false asymmetries, estimated with the help of hadron pairs ( $\pm 0.014$ ). The overall systematic uncertainty of the measured spin transfer is thus estimated to be  $\pm 0.03$ .

As the measured value for  $D_{LL'}^{\Lambda}$  shows no significant dependence on the choice of the longitudinal spin-quantization axis, the results of this section can be summarized by a single value:

$$D_{LL'}^{\Lambda} = 0.11 \pm 0.10 \text{ (stat)} \pm 0.03 \text{ (syst)}. \quad (13)$$

This represents the spin transfer to the  $\Lambda^0$  along its momentum direction, averaged over the kinematic region with  $Q^2 > 0.8 \text{ GeV}^2$ ,  $y < 0.85$ , and  $x_F > 0$ . The average fractional energy of the  $\Lambda^0$  hyperons in this sample is  $\langle z \rangle = 0.45$ , the average momentum transfer  $\langle Q^2 \rangle = 2.4 \text{ GeV}^2$ , and the average Bjorken variable  $\langle x \rangle = 0.088$ .

### C. Dependence of $D_{LL'}^{\Lambda}$ on $z$ and $x_F$

The dependence of  $D_{LL'}^{\Lambda}$  on the energy fraction  $z$  with the requirement of  $x_F > 0$  imposed is presented in Fig. 4 and Table II. As the values measured in all bins are consistent for the two axis choices, only the results for axis 1 are displayed in Fig. 4. Superimposed on the data are the phenomenological model calculations of Ref. [5] (pQCD and quark-diquark models) which predict a pronounced rise of the spin transfer at high values of  $z$ , and those of the model of Ref. [28] (SU(3)-flavor rotation of proton values) which predicts a more gradual increase. Although the data presented here extend to the highest values of  $z$  yet explored in deep-inelastic scattering, they display no evidence of a strong kinematic dependence. One should remember, however, that in the theoretical models discussed above, the  $\Lambda^0$  hyperon is assumed to be produced directly from the polarized struck quark, i.e., the contribution from the heavier hyperon decays is not included in these models (see subsection D).

The HERMES results as a function of  $x_F$  are presented in Fig. 5 and Table III.

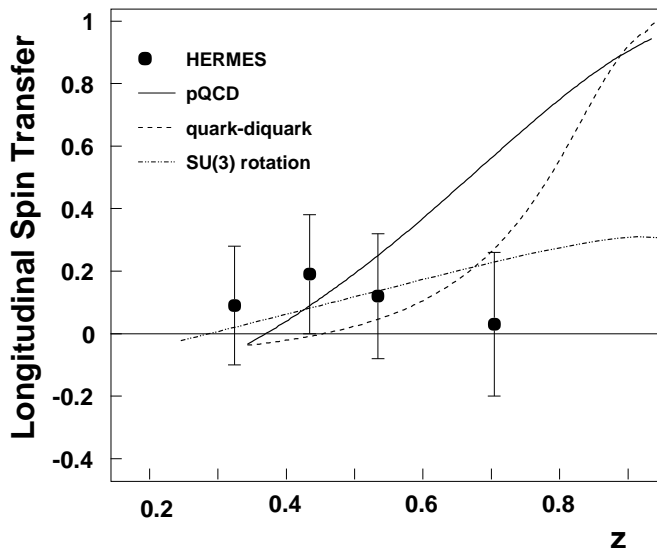


FIG. 4: Dependence of the longitudinal spin-transfer coefficient  $D_{LL'}^{\Lambda}$  on  $z$ , for  $x_F > 0$ . The curves represent the phenomenological model calculations of Refs. [5, 28], as described in the text. Error bars are statistical only.

$z$ -range	$\langle z \rangle$	$D_{LL'}^{\Lambda}$ , axis 1	$D_{LL'}^{\Lambda}$ , axis 2
$0.05 < z < 0.34$	0.28	$0.09 \pm 0.19$	$0.06 \pm 0.20$
$0.34 < z < 0.44$	0.39	$0.19 \pm 0.19$	$0.21 \pm 0.19$
$0.44 < z < 0.55$	0.49	$0.12 \pm 0.20$	$0.13 \pm 0.20$
$0.55 < z < 1$	0.66	$0.03 \pm 0.23$	$-0.02 \pm 0.23$

TABLE II: Measured values of  $D_{LL'}^{\Lambda}$  in bins of  $z$ , for  $x_F > 0$ . The quoted uncertainties are statistical only. The systematic uncertainties are on the level of  $\pm 0.03$ , as discussed in the text.

In order to provide a comparison with other deep-inelastic scattering experiments, and to illustrate the level of agreement in the region of overlap, the HERMES data are shown in Fig. 5 together with data obtained by the NOMAD experiment [14] at CERN with a 43 GeV  $\nu_{\mu}$ -beam. Results from the Fermilab E665 experiment [16] obtained with a 470 GeV polarized muon beam are also shown.

The most precise data are the charged-current  $\nu_{\mu}N \rightarrow \mu\Lambda^0 X$  measurements from NOMAD. The energy of the NOMAD neutrino beam is similar to the 27.6 GeV positron beam of the HERMES experiment. However, the spin-transfer coefficient  $D_{LL'}^{\Lambda}$  presented by HERMES cannot be immediately compared to the longitudinal  $\Lambda^0$  polarization measured by NOMAD. In the framework of the quark-parton model the polarization for the charged-

$x_F$ -range	$\langle x_F \rangle$	$D_{LL'}^{\Lambda}$ , axis 1	$D_{LL'}^{\Lambda}$ , axis 2
$-0.2 < x_F < 0.06$	-0.05	$-0.12 \pm 0.23$	$-0.16 \pm 0.23$
$0.06 < x_F < 0.24$	0.15	$0.24 \pm 0.18$	$0.24 \pm 0.18$
$0.24 < x_F < 0.42$	0.32	$0.06 \pm 0.16$	$0.08 \pm 0.16$
$0.42 < x_F < 0.56$	0.48	$0.30 \pm 0.26$	$0.33 \pm 0.26$
$0.56 < x_F < 1$	0.66	$0.09 \pm 0.34$	$-0.13 \pm 0.34$

TABLE III: Measured values of  $D_{LL'}^{\Lambda}$  in bins of  $x_F$ . The quoted uncertainties are statistical only. The systematic uncertainties are on the level of  $\pm 0.03$ , as discussed in the text.

current  $\nu_{\mu}$  interaction may be expressed as [14]:

$$P_{\Lambda}^{\nu}(x, y, z) = - \frac{q_d(x) G_{1,u}^{\Lambda}(z) - (1-y)^2 q_{\bar{u}}(x) G_{1,\bar{d}}^{\Lambda}(z)}{q_d(x) D_{1,u}^{\Lambda}(z) + (1-y)^2 q_{\bar{u}}(x) D_{1,\bar{d}}^{\Lambda}(z)}. \quad (14)$$

(Here,  $q_d(x)$  and  $q_{\bar{u}}(x)$  represent the number densities for quarks and antiquarks separately, contrary to the convention used in the rest of the paper.) The quantity  $-P_{\Lambda}^{\nu}$  thus represents the spin-transfer  $D_{LL'}^{\Lambda}$  from a struck quark to a  $\Lambda^0$  hyperon, but for a different mixture of quark flavors than in deep-inelastic scattering with electron or muon beams. However, as the NOMAD measurements were found to be nearly independent of the variable  $y$ , the interaction with  $d$  quarks (which converts  $d$  quarks to  $u$  quarks) apparently dominates over the interaction with  $\bar{u}$  quarks. Hence,  $-P_{\Lambda}^{\nu} \approx G_{1,u}^{\Lambda}/D_{1,u}^{\Lambda}$ , i.e., the NOMAD result approximately measures the spin transfer from  $u$  quarks to  $\Lambda^0$  hyperons. As  $\Lambda^0$  production at HERMES is also dominated by  $u$  quark fragmentation,  $-P_{\Lambda}^{\nu}$  from NOMAD can be qualitatively compared to  $D_{LL'}^{\Lambda}$  from HERMES. As shown in Fig. 5, the NOMAD and HERMES results are indeed compatible in the kinematic region of overlap,  $-0.2 < x_F < 0.3$ . For  $x_F > 0$  with average  $\langle x_F \rangle = 0.21$  NOMAD has obtained  $-P_{\Lambda}^{\nu} = 0.09 \pm 0.06$  (stat)  $\pm 0.03$  (syst) which is in very good agreement with the HERMES spin transfer for  $x_F > 0$  averaged over the kinematics of the experiment ( $\langle x_F \rangle = 0.31 \pm 0.01$ ):  $D_{LL'}^{\Lambda} = 0.11 \pm 0.10$  (stat)  $\pm 0.03$  (syst).

All theoretical investigations agree that the  $\Lambda^0$  production mechanisms for  $x_F > 0$  and  $x_F < 0$  are different in nature. For  $x_F < 0$  the average NOMAD result is  $-P_{\Lambda}^{\nu} = 0.21 \pm 0.04$  (stat)  $\pm 0.03$  (syst), thus showing a trend towards higher positive values at negative  $x_F$ . This behavior might suggest a change in the dominant reaction mechanism for  $\Lambda^0$  production between the current and target-fragmentation regions, as discussed in Ref. [15].

## D. Discussion

The observation of a small value of  $D_{LL'}^{\Lambda}$  points to the dominance of scattering from  $u$  or  $d$  quarks whose polar-

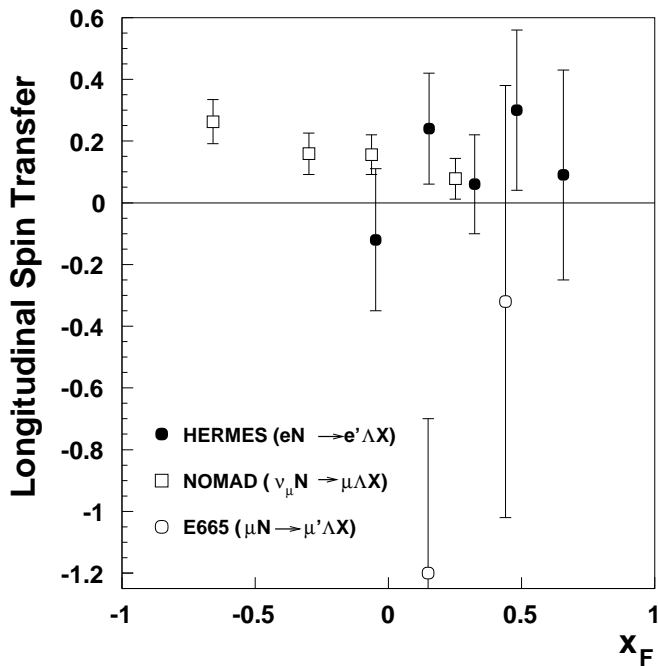


FIG. 5: Dependence of the longitudinal spin-transfer coefficient  $D_{LL'}^{\Lambda}$  on  $x_F$ . The HERMES measurements are represented by the solid circles, while the open symbols represent data from NOMAD [14] (squares) and E665 [16] (circles). Error bars are statistical only. As explained in the text, for the neutrino-induced NOMAD data the quantity plotted is  $-P_{\Lambda}^{\nu}$ .

ization within the  $\Lambda^0$  hyperons is expected to be small, although the condition  $\Delta q_u^{\Lambda} = \Delta q_d^{\Lambda} \equiv 0$  does not necessarily mean that the spin-transfer coefficient vanishes. Further, according to estimates in the framework of the Lund-based Monte Carlo model, the fraction of  $\Lambda^0$ s produced via heavier hyperon decays is significant, and complicates the production process: only about 40% of the  $\Lambda^0$  hyperons are produced directly from string fragmentation within the  $z < 0.7$  kinematic range which dominates the statistics of the present measurement. The  $\Lambda^0$  hyperons produced via  $\Sigma^0$ ,  $\Sigma^*$  or  $\Xi$  decay (no other hyperons were found to contribute significantly) may be polarized if their hyperon parents were produced polarized. For example, the average polarization of the  $\Lambda^0$  produced in the  $\Sigma^0 \rightarrow \Lambda^0 \gamma$  decay is  $P_{\Lambda} = -\frac{1}{3}P_{\Sigma^0}$  [29]. Since the  $u$  quark is strongly polarized in the  $\Sigma^0$  hyperon, a nonzero spin transfer

$$D_{LL'}^{\Lambda}(\Lambda^0 \text{ from decay of } \Sigma^0) = -\frac{1}{3} \frac{\Delta q_u^{\Sigma^0}}{q_u^{\Sigma^0}} \quad (15)$$

is expected for this partial channel [13, 20]. As the spin structures of the various hyperons differ dramatically (e.g. in the Constituent Quark Model,  $\Delta q_u^{\Sigma^0} = +\frac{2}{3}$  while  $\Delta q_u^{\Lambda^0} = 0$ ), the contributions from heavy-hyperon decay serve to dilute any net spin transfer from the polarized struck quark to the observed  $\Lambda^0$ .

In addition, at the moderate beam energy of the HERMES experiment, a contribution from the target-fragmentation mechanism to  $\Lambda^0$  production is not excluded by the requirement  $x_F > 0$ . For some fraction of the events, the target-remnant diquark will be in a spin-1 triplet state. It will be polarized since its spin orientation is fixed by that of the struck quark. Hyperons produced due to fragmentation of the polarized diquark can therefore also be polarized, further diluting any net spin transfer to the  $\Lambda^0$ .

## V. CONCLUSIONS

The polarization transfer from a polarized beam positron to a semi-inclusively produced  $\Lambda^0$  hyperon has been studied in deep-inelastic positron scattering at the HERMES experiment. In the forward-production region  $x_F > 0$ , and averaged over the kinematics of the measured sample with  $\langle z \rangle = 0.45$  and  $\langle x_F \rangle = 0.31$ , a spin-transfer coefficient  $D_{LL'}^{\Lambda} = 0.11 \pm 0.10$  (stat)  $\pm 0.03$  (syst) was obtained. This value is in good agreement with the NOMAD result  $-P_{\Lambda}^{\nu} = 0.09 \pm 0.06$  (stat)  $\pm 0.03$  (syst) measured for  $x_F > 0$  ( $\langle x_F \rangle = 0.21$ ).

The HERMES data presented here are the most precise measurements to date of spin transfer in deep-inelastic scattering at large  $x_F$ . The finding of a spin-transfer coefficient consistent with zero is in marked contrast with the large  $\Lambda^0$  polarization observed in  $e^+e^-$  annihilation at OPAL and ALEPH. This difference is not unexpected, as  $\Lambda^0$  production in the reaction  $e^+e^- \rightarrow Z^0 \rightarrow \Lambda^0 X$  is dominated by the fragmentation of strange quarks, while in deep-inelastic scattering the fragmentation of  $u$  and  $d$  quarks, weakly polarized in the  $\Lambda^0$  hyperon, is the principal source.

The small spin transfer may also be observed in deep-inelastic scattering at moderate values of  $z$  because of dilution of  $D_{LL'}^{\Lambda}$  due to a significant fraction of  $\Lambda^0$  hyperons being produced via unpolarized quarks. Although in the kinematic domain explored experimentally no significant dependence of the spin transfer on either  $z$  or  $x_F$  is observed, the moderate rise of  $D_{LL'}^{\Lambda}$  at high  $z$  predicted in Refs. [6, 28] is not excluded by the present data.

We gratefully acknowledge the DESY management for its support and the staff at DESY and the collaborating institutions for their significant effort. This work was supported by the FWO-Flanders, Belgium; the Natural Sciences and Engineering Research Council of Canada; the National Natural Science Foundation of China; the Alexander von Humboldt Stiftung; the German Bundesministerium für Bildung und Forschung (BMBF); the Deutsche Forschungsgemeinschaft (DFG); the Italian Istituto Nazionale di Fisica Nucleare (INFN); the MEXT, JSPS, and COE21 of Japan; the Dutch Foundation for Fundamenteel Onderzoek der Materie (FOM); the U. K.

Engineering and Physical Sciences Research Council, the Particle Physics and Astronomy Research Council and the Scottish Universities Physics Alliance; the U. S. Department of Energy (DOE) and the National Science Foundation (NSF); the Russian Academy of Science and the Russian Federal Agency for Science and Innovations and the Ministry of Trade and Economical Development and the Ministry of Education and Science of Armenia.

- 
- [1] B.W. Filippone and X.-D. Ji, *Adv. Nucl. Phys.* **26**, 1 (2001).
- [2] M. Burkardt and R.L. Jaffe, *Phys. Rev. Lett.* **70**, 2537 (1993).
- [3] QCDSF Collaboration, M. Göckeler et al., *Phys. Lett. B* **545**, 112 (2002).
- [4] HERMES Collaboration, A. Airapetian et al., *Phys. Rev. Lett.* **92**, 012005 (2004); *Phys. Rev. D* **71**, 012003 (2005).
- [5] B.-Q. Ma, J.-J. Yang, I. Schmidt, *Phys. Lett. B* **477**, 107 (2000).
- [6] C. Boros, J.T. Londergan, and A.W. Thomas, *Phys. Rev. D* **61**, 014007 (2000).
- [7] C. Liu and Z. Liang, *Phys. Rev. D* **62**, 094001 (2000).
- [8] R.L. Jaffe, *Phys. Rev. D* **54**, 6581 (1996).
- [9] P.J. Mulders and R.D. Tangerman, *Nucl. Phys. B* **461**, 197 (1996).
- [10] A. Kotzinian, A. Bravar, D. von Harrach *Eur. Phys. J. C* **2**, 329 (1998).
- [11] OPAL Collaboration, K. Ackerstaff et al., *Eur. Phys. J. C* **2**, 49 (1998).
- [12] ALEPH Collaboration, D. Buskulic et al., *Phys. Lett. B* **374**, 319 (1996).
- [13] G. Gustafson and J. Häkkinen, *Phys. Lett. B* **303**, 350 (1993).
- [14] NOMAD Collaboration, P. Astier et al., *Nucl. Phys. B* **588**, 3 (2000).
- [15] J. Ellis, D. Kharzeev, and A. Kotzinian, *Zeit. Phys. C* **69**, 467 (1996).
- [16] E665 Collaboration, M.R. Adams et al., *Eur. Phys. J. C* **17**, 263 (2000).
- [17] HERMES Collaboration, A. Airapetian et al., *Phys. Rev. D* **64**, 112005 (2001).
- [18] CLAS Collaboration, D.S. Carman et al., *Phys. Rev. Lett.* **90**, 131804 (2003).
- [19] N. Akopov et al., *Nucl. Instrum. Methods A* **479**, 511 (2002).
- [20] D. Ashery and H.J. Lipkin, *Phys. Lett. B* **469**, 263 (1999).
- [21] V.N. Gribov and L.N. Lipatov, *Phys. Lett. B* **37**, 78 (1971).
- [22] D.P. Barber et al., *Phys. Lett. B* **343**, 436 (1995).
- [23] HERMES Collaboration, K. Ackerstaff et al., *Nucl. Instrum. Methods A* **417**, 230 (1998).
- [24] V. Andreev et al., *Nucl. Instrum. Methods A* **465**, 482 (2001).
- [25] D. Barber et al., *Nucl. Instrum. Methods A* **329**, 79 (1993); *Nucl. Instrum. Methods A* **338**, 166 (1994).
- [26] M. Beckmann et al., *Nucl. Instrum. Methods A* **479**, 334 (2002).
- [27] S. Belostotski in *Proc. of the IX-Workshop on High Energy Spin Physics (SPIN-01), Dubna 2001*, preprint JINR E1,2-2002-103, 192 (2002).
- [28] B.-Q. Ma, I. Schmidt, J. Soffer, and J.-J. Yang, *Phys. Rev. D* **65**, 034004 (2002).
- [29] R. Gatto, *Phys. Rev.* **109**, 610 (1958).